DVB-S2: The Second Generation Standard for Satellite Broad-band Services

ALBERTO MORELLO AND VITTORIA MIGNONE

Invited Paper

DVB-S2 is the second-generation specification for satellite broad-band applications, developed by the Digital Video Broadcasting (DVB) Project in 2003. The system is structured as a toolkit to allow the implementation of the following satellite applications: TV and sound broadcasting, interactivity (i.e., Internet access), and professional services, such as TV contribution links and digital satellite news gathering. It has been specified around three concepts: best transmission performance approaching the Shannon limit, total flexibility, and reasonable receiver complexity. Channel coding and modulation are based on more recent developments by the scientific community: low density parity check codes are adopted, combined with QPSK, 8PSK, 16APSK, and 32APSK modulations for the system to work properly on the nonlinear satellite channel. The framing structure allows for maximum flexibility in a versatile system and also synchronization in worst case configurations (low signal-to-noise ratios). Adaptive coding and modulation, when used in one-to-one links, then allows optimization of the transmission parameters for each individual user, dependant on path conditions. Backward-compatible modes are also available, allowing existing DVB-S integrated receivers–decoders to continue working during the transitional period. The paper provides a tutorial overview of the DVB-S2 system, describing its main features and performance in various scenarios and applications.

Keywords*—Adaptive coding and modulation (ACM), digital satellite news gathering (DSNG), DVB-S2, low density parity check (LDPC) coding, satellite broadcasting.*

I. INTRODUCTION

The Digital Video Broadcasting (DVB) Project is an industry-led consortium of over 260 broadcasters, manufacturers, network operators, software developers, regulatory bodies, and others in over 35 countries, committed to designing technical specifications for the global delivery of digital television and data services. It was formed in September 1993, and at the end of the same year produced its first specification, DVB-S [1], the satellite delivery specification now used by most satellite broadcasters around the world for DTH (direct-to-home) television services. The DVB-S system is based on QPSK modulation and convolutional forward error correction (FEC), concatenated with Reed–Solomon coding. Since then, DVB-S links also started to be proposed for professional point-to-point transmission of television programs, to convey directly to the broadcaster's premises audio/video material originated in the studios (TV contribution) and/or from remote locations by outside broadcasting vans or portable uplink terminals [digital satellite news gathering (DSNG)], without requiring a local access to the fixed telecom network. In 1998, DVB produced its second standard for satellite applications, DVB-DSNG [2], extending the functionalities of DVB-S to include higher order modulations (8PSK and 16QAM) for DSNG and other TV contribution applications by satellite.

In the last decade, studies in the field of digital communications and, in particular, of error correcting techniques suitable for recursive decoding, have brought new impulse to the technology innovations. The results of this evolutionary trend, together with the increase in the operators' and consumers' demand for larger capacity and innovative services by satellite, led DVB to define in 2003 the second-generation system for satellite broad-band services, DVB-S2 [3], now recognized as ITU-R and European Telecommunications Standards Institute (ETSI) standards.

The system has been designed for different types of applications:

- broadcasting of standard definition and high-definition TV (SDTV and HDTV);
- interactive Services, including Internet access, for consumer applications (for integrated receivers–decoders (IRDs) and personal computers);
- professional applications, such as digital TV contribution and news gathering;
- data content distribution and Internet trunking.

Manuscript received January 19, 2005; revised August 3, 2005.

The authors are with the Research and Technology Innovation Centre, RAI, Torino 10135, Italy (e-mail: a.morello@rai.it).

Digital Object Identifier 10.1109/JPROC.2005.861013

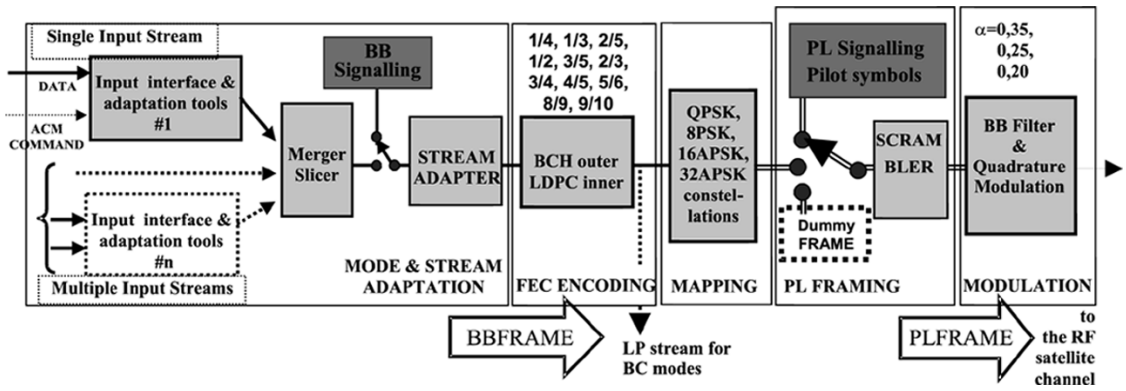

Fig. 1. Functional block diagram of the DVB-S2 transmission system.

To be able to cover all the application areas while still keeping the single-chip decoder at reasonable complexity levels, DVB-S2 is structured as a *toolkit*, thus also enabling the use of mass market products for professional or *niche* applications.

The DVB-S2 standard has been specified around three key concepts: best transmission performance, total flexibility, and reasonable receiver complexity. To achieve the best performance-complexity tradeoff, quantifiable in about 30% capacity gain over DVB-S, DVB-S2 benefits from more recent developments in channel coding and modulation. For interactive point-to-point applications such as IP unicasting, the adoption of the adaptive coding and modulation (ACM) functionality allows optimization of the transmission parameters for each individual user on a frame-by-frame basis, dependent on path conditions, under closed-loop control via a return channel (connecting the IRD/PC to the DVB-S2 uplink station via terrestrial or satellite links, signaling the IRD/PC reception condition). This results in a further increase in the spectrum utilization efficiency of DVB-S2 over DVB-S, allowing the optimization of the space segment design, thus making possible a drastic reduction in the cost of satellite-based IP services.

DVB-S2 is so flexible that it can cope with any existing satellite transponder characteristics, with a large variety of spectrum efficiencies and associated SNR requirements. Furthermore it is designed to handle a variety of advanced audio–video formats which the DVB Project is currently defining [5]. DVB-S2 accommodates any input stream format, including single or multiple MPEG transport streams (TSs) (characterized by 188-byte packets), IP as well as ATM packets, continuous bit-streams.

In the following sections of the paper, the DVB-S2 system architecture and performance will be discussed: Section II describes the transmission system structure, Section III presents a possible receiver implementation, Section IV gives the system performance in the ideal additive white Gaussian noise (AWGN) channel and in a typical nonlinear satellite environment, while Section V shows the excellence of DVB-S2 when compared with DVB-S and DVB-DSNG, for various different applications. Finally, conclusions are drawn in Section VI.

II. The System Block Diagram

The DVB-S2 transmission system is structured as a sequence of functional blocks, schematically represented in Fig. 1 [6].

Signal generation is based on two levels of framing structures:

— BBFRAME at base-band (BB) level, carrying a variety of signaling bits, to configure the receiver flexibly according to the application scenario;

— PLFRAME at physical layer (PL) level, carrying few highly protected signaling bits, to provide robust synchronization and signaling at the physical layer.

A. Mode and Stream Adaptation

Depending on the application, DVB-S2 input sequences may be single or multiple MPEG TSs, single or multiple generic streams, either packetized or continuous. Mode and stream adaptation blocks provide input stream interfacing, synchronization, and other optional tools required for ACM, and CRC coding for error detection in the receiver at packet level (not active for continuous streams).

Furthermore, for multiple inputs, it provides merging of input streams in a single transmission signal and slicing in FEC code blocks (identified as data blocks), composed of bits taken from a single input port, to be transmitted in a homogeneous transmission mode (FEC code and modulation). Then base-band frames BBFRAME are built by appending the base-band header (80 bits) in front of the data block, to notify the receiver of the input stream format and Mode Adaptation type: single or multiple input streams, generic or TS, constant coding and modulation (CCM) or ACM, and many other configuration details. Thanks to the FEC protection (covering both the header and the data payload) and the wide length of the FEC frame, the base-band header can in fact contain many signaling bits without losing transmission efficiency or ruggedness against noise.

In case the user data available for transmission are not sufficient to completely fill a BBFRAME, padding bits are also inserted to complete it. Finally, base-band scrambling is performed.

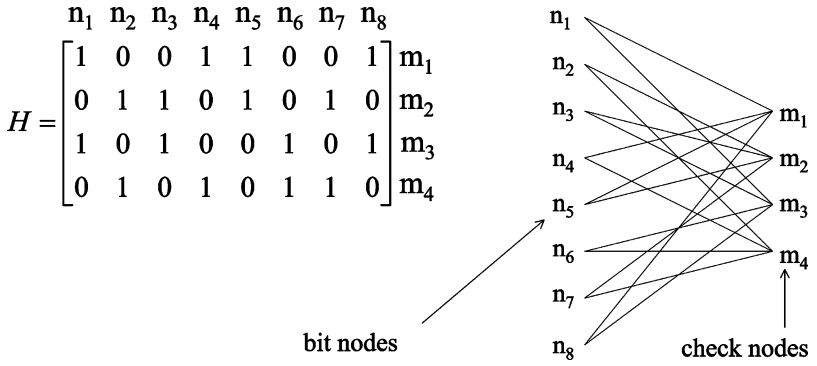

Fig. 2. Parity check matrices and corresponding bipartite graph of an LDPC code.

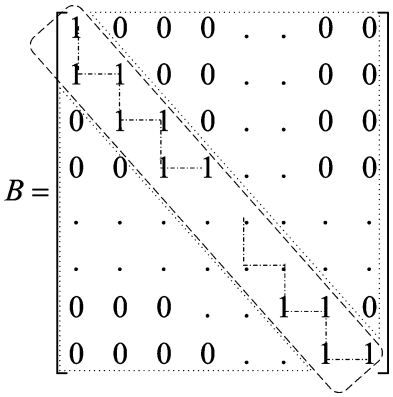

Fig. 3. Staircase lower triangular submatrix of the parity check matrix.

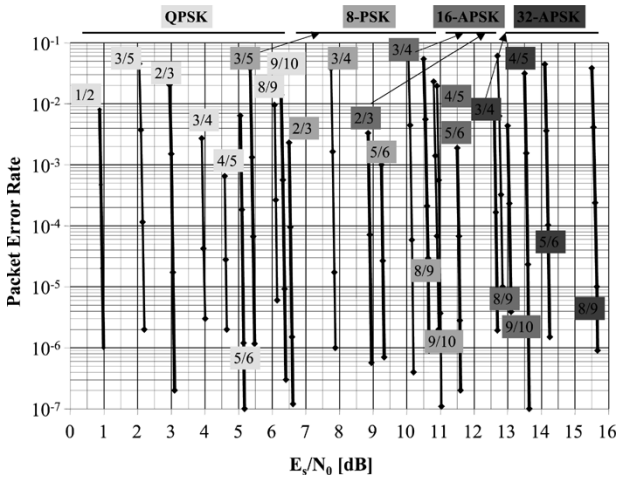

Fig. 4. DVB-S2 FEC (BCH&LDPC) performance in the AWGN channel: various code rates and modulation configurations are considered for coded blocks of 64 800 bits. Es/No is the SNR after the receiving matched filter.

B. FEC Encoding

The FEC, together with the modulation, is the key subsystem to achieve excellent performance by satellite, in the presence of high levels of noise and interference. The DVB-S2 FEC selection process, based on computer simulations, compared seven proposals over the AWGN channel—parallel or serially concatenated convolutional codes, product codes, low density parity check codes (LDPC)—all using "turbo" (i.e., recursive) decoding techniques. The winning system was based on LDPC codes, and offered the minimum distance from the Shannon limit in the linear AWGN channel, under the constraint of maximum decoder complexity of 14 mm^2 of silicon (0.13-μm technology).

LDPC codes were discovered by R. G. Gallager [7] in 1960, but technology at that time was not mature enough for efficient implementation. The success of iterative decoding motivated MacKay and Neal to repropose them in 1995 [8], [9].

LDPC codes are linear block codes characterized by sparse parity check matrices $H_{(N-K)\times N}$, where each block of K information bits are encoded to a codeword of size N. They can be equivalently represented by the bipartite graph which connects each check equation (check node, $N-K$) to its participating bits (bit nodes, N). The number of edges adjacent to a node is called the *degree* of that node.

An example LDPC code of codeword size $N=8$ and rate 1/2 ($K=4$) is presented in Fig. 2.

LDPC codes have an easily parallelizable decoding algorithm, consisting of simple operations such as additions, comparison, and table look-up, which makes them suitable for iterative decoding at reasonable complexity.

To reduce the encoding complexity, the LDPC codes standardized by DVB-S2 [10] are characterized by parity check matrices of the form $H_{(N-K)\times N} = A_{(N-K)\times K} B_{(N-K)\times(N-K)}$, where B is staircase lower triangular (Fig. 3).

Furthermore, to reduce the storage requirements, a periodicity $M=360$ has been introduced on H. For a group of M bit nodes, if the check nodes connected to the first bit node, of degree d_v, are $\{c_1, c_2, \ldots, c_{d_v}\}$, then the check nodes connected to the ith bit node ($i \leq M$) are numbered as

$$\{c_1+(i-1)q\} \bmod (N-K), \{c_2+(i-1)q\} \bmod (N-K), \ldots, \{c_{d_v}+(i-1)q\} \bmod (N-K)$$

where $N-K$ is the total number of check nodes and $q = (N-K)/M$.

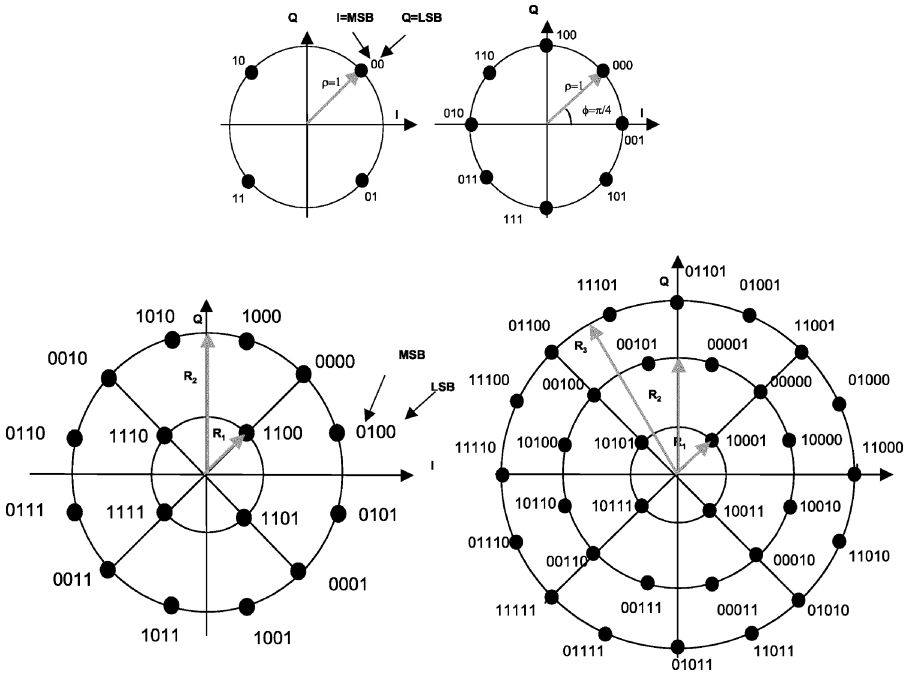

Fig. 5. The four DVB-S2 constellations before PL-scrambling.

In order to avoid possible error floors at low error rates (for which it is difficult, if not impossible, to accurately measure), concatenated BCH outer codes are introduced, with the same block length as the LDPC code and an error correction capability of 8 to 12 bits, depending on the inner LDPC code configuration.

The total BCH&LDPC block length is 64 800 bits for applications not too critical for delays, 16 200 bits otherwise. Code rates of 1/4, 1/3, 2/5, 1/2, 3/5, 2/3, 3/4, 4/5, 5/6, 8/9, and 9/10 are available depending on the selected constellation and the system application. In particular, coding rates 1/4, 1/3, and 2/5 have been introduced to operate, in combination with QPSK, under exceptionally poor link conditions, for signal to noise ratios E_s/N_0 below 0 dB.

FEC and modulation modes are constant within a frame but may be changed in different frames, when ACM is used; furthermore, the transmitted signal can contain a mix of normal and short code blocks. Bit interleaving is then applied to FEC-coded bits in 8PSK, 16APSK, and 32APSK to separate, from each other, bits mapped onto the same transmission signal.

Error rate requirements for DVB-S2 are very stringent, 10^{-7} MPEG TS packet error rate (PER), approximately corresponding to less than one erroneous packet per hour for a service bit rate of 5 Mb/s. Fig. 4 shows the excellent DVB-S2 FEC performance in the AWGN channel for various code rates and modulations, with FEC-coded blocks of 64 800 bits and less than 50 decoding iterations in the receiver (computer simulations by M. Eroz *et al.* reported in [10]). Short code blocks generally give slightly worse performance, due to the smaller frame dimension [4].

C. Mapping Into Constellations

Four modulation modes can be selected for the transmitted payload (see Fig. 5): QPSK, 8PSK, 16APSK, and 32APSK, depending on the application area. By selecting the modulation constellation and code rates, spectrum efficiencies from 0.5 to 4.5 bits per symbol are available and can be chosen dependent on the capabilities of the satellite transponder used.

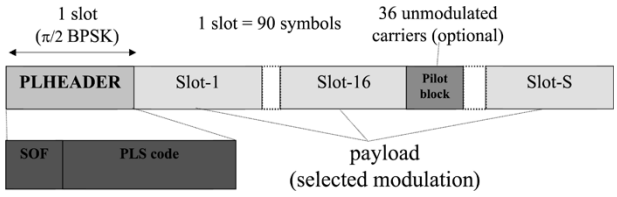

Fig. 6. PL frame scheme.

The 16APSK and 32APSK constellations have been optimized for nonlinear transponders by placing the points on circles; nevertheless their performance in the AWGN channel is comparable with those of 16QAM or 32QAM respectively [12].

QPSK and 8PSK are typically proposed for broadcast applications, since they are virtually constant envelope modulations and can be used in nonlinear satellite transponders driven near saturation. The 16APSK and 32APSK modes are mainly targeted at professional applications, due to the higher requirements in terms of available SNR, but they can also be used for broadcasting. While these modes are not as power efficient as the other modes, the spectrum efficiency is much greater. They need to operate the satellite transponder in a quasi-linear region or, alternatively, to adopt advanced predistortion methods in the uplink station to minimize the effect of transponder nonlinearity.

D. PL Framing

The physical layer signal is composed of a regular sequence of frames (Fig. 6), within which the modulation and coding scheme is homogeneous (in the ACM configuration it may change in adjacent frames). Every frame is composed of

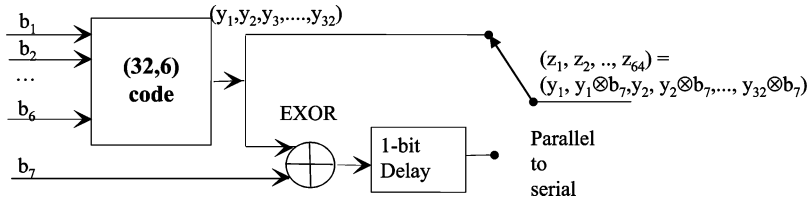

Fig. 7. PLS code construction.

a payload of 64 800 bits in the "normal frame" configuration, 16 200 bits in the "short frame" one, corresponding to a FEC code block. A header of 90 binary modulation symbols preceeds the payload, containing synchronization and signaling information, to allow a receiver to synchronize (carrier and phase recovery, frame synchronization) and detect the modulation and coding parameters before demodulation and FEC decoding.

The first 26 binary symbols (the sequence $18D2E82_{\mathrm{HEX}}$) of the PL header identify the start of the PL frame [SOF (start of frame)], the remaining 64 symbols are used for signaling the system configuration. Since the PL Header is the first entity to be decoded by the receiver, it could not be protected by the FEC scheme (i.e., BCH&LDPC). On the other hand, it had to be perfectly decodable under the worst-case link conditions (SNR of about -2.5 dB, see Fig. 22). Therefore, to minimally affect the global spectrum efficiency, the signaling information at this level has been reduced to 7 bits, 5 of which are used to indicate the modulation and coding configuration (MODCOD field), 1 for frame length (64 800 or 16 200), 1 for presence/absence of pilots to facilitate receiver synchronization (as explained below). These bits are then highly protected by an interleaved first-order Reed–Muller block code with parameters rate (64, 7, $t = 32$), suitable for soft-decision correlation decoding. The construction utilizes the first-order Reed–Muller code of parameters (32, 6, $t = 16$), whose generator matrix is

$$\begin{array}{c}
01\,010\,101\,010\,101\,010\,101\,010\,101\,010\,101 \\
00\,110\,011\,001\,100\,110\,011\,001\,100\,110\,011 \\
00\,001\,111\,000\,011\,110\,000\,111\,100\,001\,111 \\
00\,000\,000\,111\,111\,110\,000\,000\,011\,111\,111 \\
00\,000\,000\,000\,000\,001\,111\,111\,111\,111\,111 \\
11\,111\,111\,111\,111\,111\,111\,111\,111\,111\,111
\end{array}.$$

The generator matrix can be constructed recursively by the well-known $|\boldsymbol{u}|\boldsymbol{u}+\boldsymbol{v}|$ construction. This notation indicates how to use two codes of length n to construct a code of length $2n$, i.e., $\boldsymbol{u}$ and $\boldsymbol{v}$ are drawn from each of the component codes respectively. In the case of a first-order Reed–Muller code, $\boldsymbol{v}$ uses the trivial linear code $\mathbf{0}$ and $\mathbf{1}$, the all-zero and all-one vectors of length n, as code words, and $\mathbf{u}$ belongs to a first-order Reed–Muller code of length n.

The formulation of a PL signaling code (PLS) word is shown in Fig. 7. For seven information bits, the first six bits are encoded by the (32, 6, $t = 16$) first-order Reed–Muller code to obtain the binary vector $\mathbf{Y} = (y_1, y_2, \cdots, y_{32})$. Vector $\mathbf{Y}$ is further duplicated into two identical vectors. Every bit of the first vector is binary summed with the seventh information bit, then the two vectors are multiplexed bit by bit to form a vector of length 64. In other words, let $\mathbf{Y} = (y_1, y_2, \cdots, y_{32})$ be a codeword of the first-order Reed–Muller code (32, 6, $t = 16$). Then two code words of the (64, 7, $t = 32$) code can be generated as $(y_1, y_1, y_2, y_2, \ldots, y_{32}, y_{32})$ and $(y_1, \overline{y}_1, y_2, \overline{y}_2, \ldots, y_{32}, \overline{y}_{32})$ respectively, where $\overline{y}$ represents the binary complement of y. Instead of bit-by-bit multiplexing the upper and lower vector, if the two vectors were cascaded together, it would have resulted in the $|u|u+v|$ construction of the first-order Reed–Muller code of parameters (64, 7, $t = 32$). This shows that the PLS code constructed in such a way is actually an interleaved first-order Reed–Muller code of parameters (64, 7, $t = 32$), which is known to achieve the best minimum distance for a binary (64, 7) code, therefore, the code of Fig. 7 is an optimal binary (64, 7) code.

This PLS code construction has been selected in order to obtain a useful property for frame synchronization when differential demodulation is used (see Section III-A)

$$z_{2i-1} \oplus z_{2i} = \begin{cases} 0 & if \quad z_{2i-1} = z_{2i} \\ 1 & if \quad z_{2i-1} = \overline{z}_{2i} \end{cases}, \quad \forall\, i = 1, 2, \ldots, 32. \tag{1}$$

The PLS code word is then scrambled by a 64-bit extended m-sequence, to improve its autocorrelation property.

Independently from the modulation scheme of the PLFRAME payload (FEC code block), the 90 binary symbols forming the PL header are $\pi/2$-BPSK modulated; this variant of the classical BPSK constellation introduces a $\pi/4$ rotation on even symbols and $-\pi/4$ on odd symbols, thus allowing a reduction of the radio-frequency signal envelope fluctuations.

The PL frame payload is composed of a different number of modulated symbols depending on the FEC length (64 800 or 16 200) and the modulation constellation, but (excluding the optional pilots) the payload length is always a multiple of a slot of 90 symbols (Fig. 6), thus showing periodicities which can be exploited by the frame synchronizer in the receiver: once the current PL header has been decoded, the decoder knows exactly the PL frame length and thus the position of the following SOF.

PL framing also provides for: 1) optional dummy PL frame insertion, when no useful data is ready to be sent on the channel and 2) the insertion of optional pilots to facilitate receiver synchronization. The DVB-S2 FEC codes are in fact so powerful that carrier recovery may become a serious problem for high-order modulations working at low SNRs in the presence of high levels of phase noise in consumer low noise block (LNB) converters and tuners: this is particularly the case with some low rate 8PSK, 16APSK,

and 32APSK modes of DVB-S2. Pilots are unmodulated symbols, identified by $I = Q = 1/\sqrt{2}$, grouped in blocks of 36 symbols and inserted every 16 payload slots, thus giving a maximum capacity loss of approximately 2.4% when used.

Finally, scrambling for energy dispersal is carried out to comply with the Radio Regulations for spectrum occupancy and to transmit a sort of "signature" of the service operator, for a rapid identification in case of errors in the uplink procedures.

E. Quadrature Modulation

Square-root raised cosine baseband filtering and quadrature modulation are then applied, to shape the signal spectrum and to generate the RF signal. There are three permitted values for the rolloff factor: 0.35 as in DVB-S, plus 0.25 and 0.20 for tighter bandwidth restrictions.

F. The Backward Compatible Modes

The large number of DVB-S receivers already installed makes it very difficult for many established broadcasters to think of an abrupt change of technology in favor of DVB-S2. In such scenarios, backward-compatibility may be required during the migration period, allowing legacy DVB-S receivers to continue operating, while providing additional capacity and services to new, advanced receivers. At the end of the migration process, when the complete receiver population has migrated to DVB-S2, the transmitted signal could be modified to the nonbackward compatible mode, thus exploiting the full potential of DVB-S2.

Optional backward-compatible (BC) modes have therefore been defined in DVB-S2, intended to send two MPEG TSs within a single satellite channel. The first [high priority (HP)] stream is compatible with DVB-S legacy receivers, as well as with DVB-S2 receivers, the second [low priority (LP)] stream is compatible with DVB-S2 receivers only.

In DVB-S2, backward compatibility can be implemented by hierarchical modulation [20], where the two HP and LP TSs are synchronously combined at modulation symbol level on a nonuniform 8PSK constellation (Fig. 8).

In the hierarchical modulation approach, according to Fig. 9, the LP DVB-S2 compliant signal is BCH and LDPC encoded, with LDPC code rates 1/4, 1/3, 1/2, or 3/5. Then the hierarchical mapper generates the nonuniform 8PSK constellation: the two HP DVB-S bits define a QPSK constellation point (receivable by any conventional DVB-S IRD), while the single bit from the DVB-S2 LDPC encoder sets an additional rotation $\pm\theta$ before transmission (producing a small degradation on DVB-S IRD performance, depending on the θ amplitude). Analytically, the signal at the output of the hierarchical modulator can be written as

$$v_{HM} = \sum_k A e^{j\Phi_k} s(t - kT), \tag{2}$$

where the discrete phase Φ_k takes values in the range $\{(\pi/2)l + (\pi/4) + (-1)^{l+k+1}\theta\}$ for $l = 3Q_S - 2I_S Q_S + I_S$

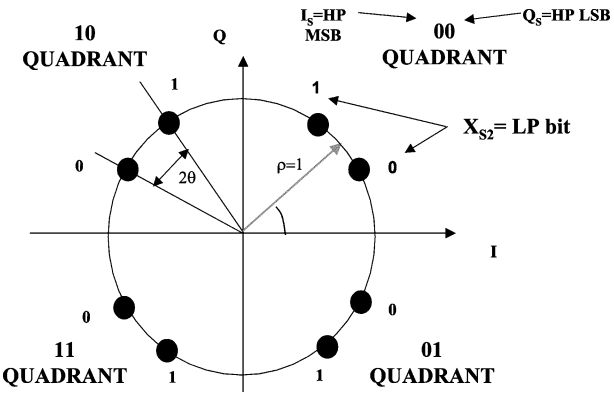

Fig. 8. Nonuniform 8PSK constellation.

(four possible values 0,1,2,3, Q_S and I_S defined in Fig. 8) and $k = X_{S2}$ (2 possible values 0, 1). Q_S, I_S and X_{S2} are defined in Fig. 8.

Since the resulting signal has a quasi-constant envelope, it can be transmitted in a single transponder driven near saturation.

III. DVB-S2 Receiver Issues

A. Synchronization

Synchronization of the DVB-S2 system at the receiver is a hard task for the following main reasons: the wide range of possible system configurations and the presence of operative modes working at very low SNRs. For ACM modes, a further difficulty is the frame-by-frame variation of the modulation scheme, and the fact that in a given receiving location the SNR may be insufficient to maintain synchronization during all frames; therefore receiver synchronization has to be acquired "on-the-fly" for the decodable frames. Furthermore, considering that the users will probably not change their outdoor units when moving from DVB-S to DVB-S2, the DVB-S2 carrier recovery algorithms should be able to cope with the less stringent LNB performance required by DVB-S QPSK modulation, with phase noise mask which could result critical for higher order modulations.

Fig. 10 gives an example schematic representation of a DVB-S2 digital demodulator, after signal down-conversion from the RF/IF front-end to baseband. There now follows a description of example synchronization subsystems, as proposed in [11] and [16] to coherently demodulate the received signal, before passing it to the FEC decoder. Other less-sophisticated synchronization schemes, not requiring the transmission of pilots, may be used for noncritical DVB-S2 modes.

1) Clock Recovery: Clock recovery can be performed first in the acquisition phase by using the well-known (nondata aided) Gardner's algorithm [15], whose performance, over the range of E_s/N_0 of interest for DVB-S2, is quite insensitive to the modulation format and to a carrier frequency error of up to 0.1–0.2 times the symbol rate. The target lock-in frequency error assumed for DVB-S2 services is 5 MHz, corresponding to 20% of the symbol rate at 25 Mbaud. To make the system work with the same initial frequency error, and

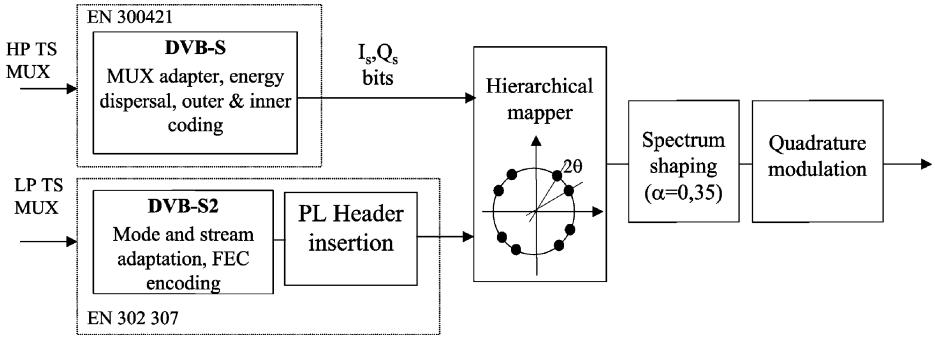

Fig. 9. Functional block diagram of hierarchical backward-compatible DVB-S2 system.

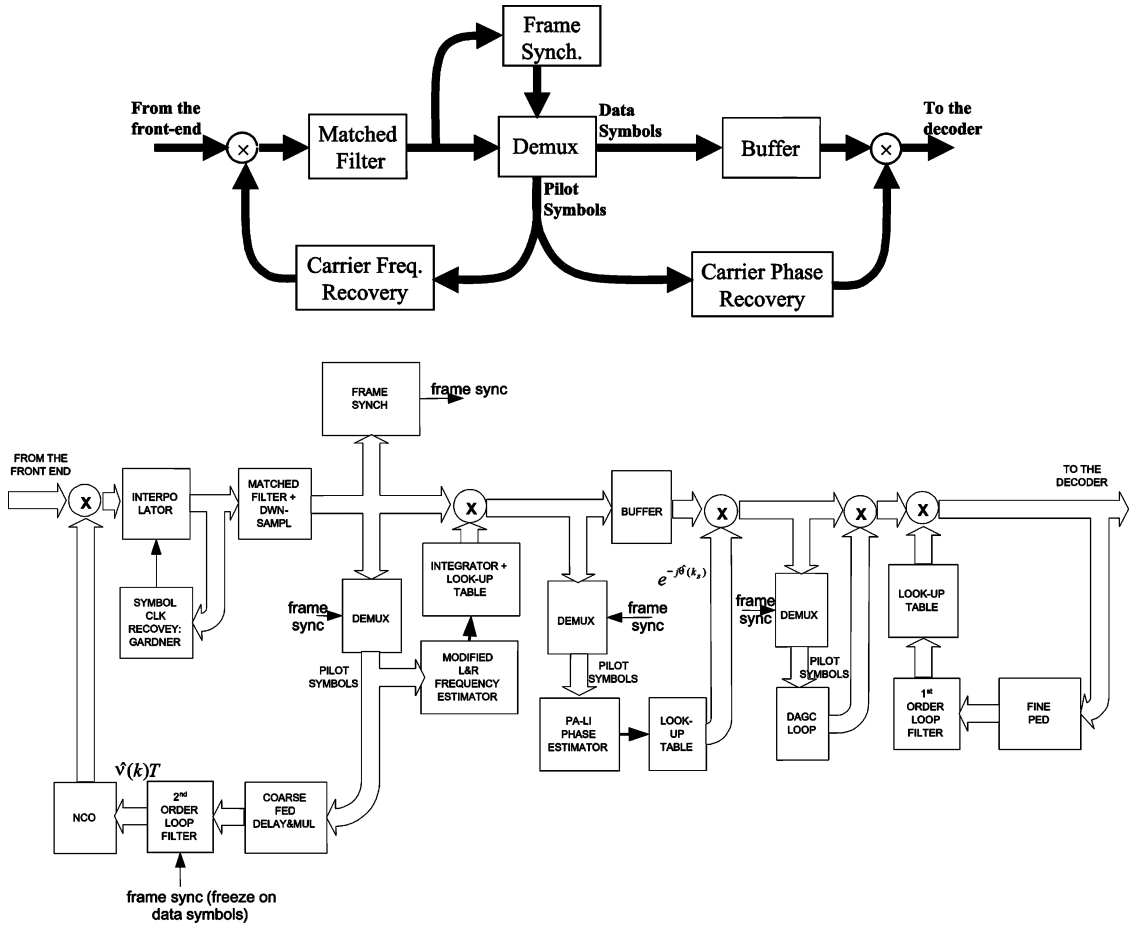

Fig. 10. Simplified (upper) and detailed (lower) block diagrams of the DVB-S2 digital demodulator.

also for lower symbol rates (down to 10 Mbaud), two timing recovery algorithms can be run in parallel—the first with a signal prerotated in frequency by $+1/4$ of the symbol rate R_s and the second by $-1/4R_s$, with selection of the converged output after a predetermined transient time. The rms jitter of the algorithm worsens as the system rolloff factor decreases: for the DVB-S2 range of rolloff and E_s/N_0, a normalized (to the symbol rate) loop bandwidth of $5{\cdot}10^{-5}$ seems to be required for negligible impact on the receiver performance. With this loop bandwidth and using a second-order loop, a clock frequency error of 10 ppm can be tracked with no residual error bias. Also, the overall acquisition transient of the timing recovery unit would be around 10^5 symbols, which corresponds to about 4 ms at 25 Mbaud. Timing adjustment can then be carried out through a digital interpolator (typically implemented as a parabolic or cubic interpolator, in order to limit the distortions to a minimum). Matched filtering follows, at two samples per symbol.

2) Physical Layer Frame Synchronization: When pilots are used for carrier/phase recovery, Physical Layer frame synchronization is the next step to be performed after symbol timing recovery, in order to be able to locate the pilots. The possibility of using the SOF sequence alone for PL frame synchronization has been investigated, but it turned out to be too short to provide reliable convergence at low SNRs. Since coherent demodulation is not yet possible at this step, the differential correlation scheme of Fig. 11 is proposed in [16], based on the 90 SOF and PLS symbols of the PL header. The 89 shift registers in the circuit can be separated into two groups—the first (25 shift registers) associated with SOF

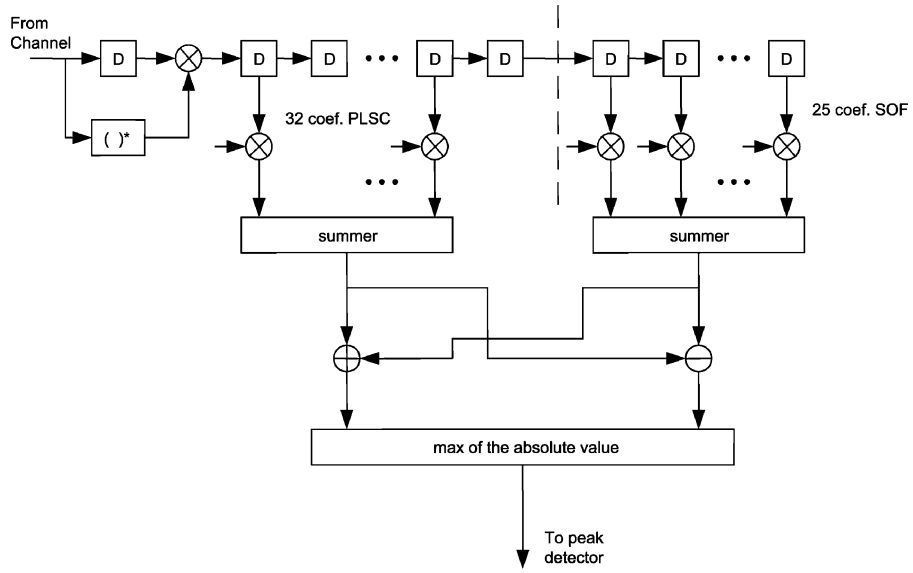

Fig. 11. Differentially coherent detection of the SOF and PLS symbols.

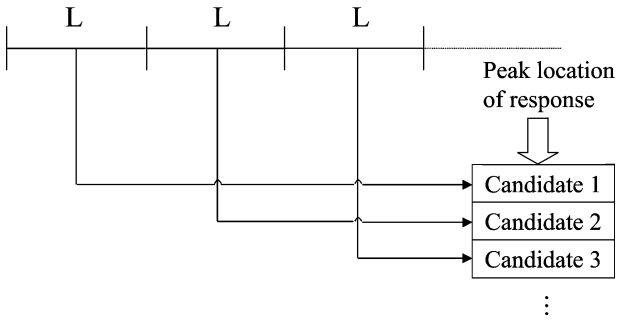

Fig. 12. Frame synchronization peak detector.

symbols, and the second (64 shift registers) with PLS symbols. The corresponding taps are 57, since in the second part, only 32 out of the 64 differentials are known at the receiver [property (1)]. The shift register contents are multiplied by the taps, then summed. The maximum of the absolute value of the two summing devices is the output of the correlation circuit, to be further processed by a peak search algorithm, comparing it to a predetermined threshold, which must be accurately designed in order to balance the probabilities of missed detection and false alarms.

To improve the performance of the algorithm of Fig. 11, successive PL headers may be detected, as proposed in [16] and [4]. In DVB-S2 the PL frame lengths depend on the modulation adopted and the presence/absence of pilots. Therefore, they are constant in CCM modes, while they change frame-by-frame in ACM modes. In [16] a simple peak search algorithm within a prescribed window is proposed for CCM, provided that the search window is big enough to contain at least one PL header. Since, from a performance perspective, the dimension L of the search window should be as small as possible, it should be defined according to the lowest modulation order considered, i.e., QPSK, meaning that L should be larger than $32\,400 + 90$ ($+792$ if pilots are present) for 64 800-bit frames.

Fig. 12 shows the proposed peak search diagram. Given the above considerations on the length L of the search window, each block of L symbols could contain multiple PL headers: the location in each block of the maximum peak is a "candidate," and in CCM modes a simple analysis on the candidate periodicity can allow the identification of the frame synchronization.

In the case of ACM there is no periodicity in the SOF position; therefore, it is necessary to decode PLS to determine the position of the next SOF. For the algorithm of Fig. 12, the PLS code of a candidate is decoded, and if the correlation at the next SOF and PLC is of sufficient strength, the receiver will declare a successful frame synchronization; otherwise, the receiver will proceed to check the next candidate.

Simulations [16] indicate that the mean acquisition time is around 20 ms for 25-Mbaud transmissions at $E_s/N_0 = -2$ dB and less than 4 ms at $E_s/N_0 = 0.7$ dB (these numbers being approximately the operating E_s/N_0 values for QPSK 1/4 and QPSK 1/2 respectively, in the AWGN channel). At 99% probability the acquisition time for frame synchronization is around 130 ms at -2 dB and 10 ms at 0.7 dB.

An alternative algorithm for ACM, described by the finite-state machine of Fig. 13, is proposed in [4], also showing good performance in the presence of poor channel SNRs.

3) Coarse Carrier Frequency Recovery: For the target lock-in frequency error range of 5 MHz, a simple pilot-aided carrier recovery technique is proposed in [11] to be implemented in a feedback structure, with an NCO driven by a second-order loop filter fed by a frequency error detector (FED) that implements the following equation [13]:

$$e(k) = \mathrm{Im}\left\{z^{(p)}(k) \cdot c^{(p)*}(k) \cdot z^{(p)*}(k-2) \cdot c^{(p)}(k-2)\right\} \tag{3}$$

where $z^{(p)}(k)$ are the signal samples at the matched filter output corresponding to the pilots $c^{(p)}(k)$. The loop is active only during the pilots reception and is frozen (i.e., the value of the frequency estimate is kept constant) during the data symbols.

Simulations in [11] indicate that for the worst case and with the required range of E_s/N_0, this synchronizer is able

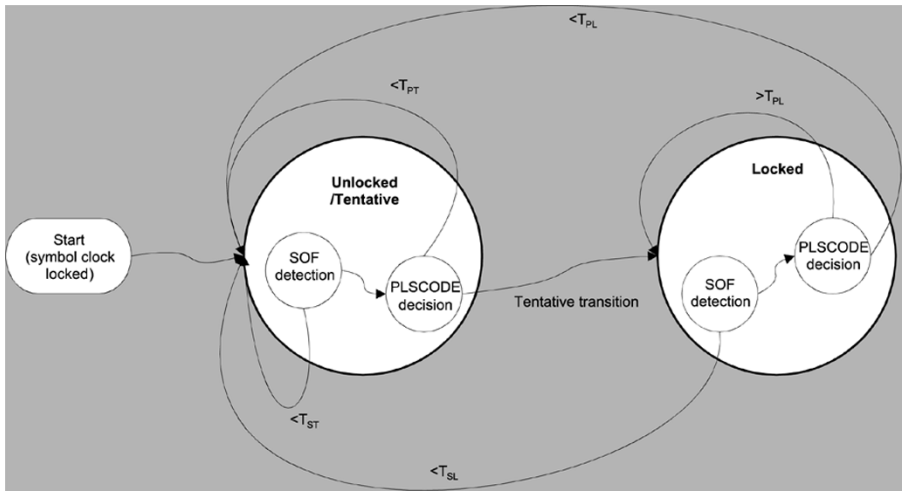

Fig. 13. Finite-state machine for PL frame acquisition.

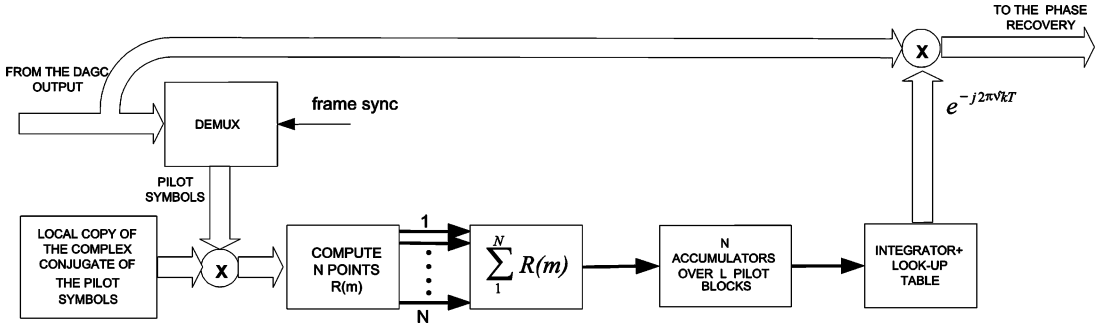

Fig. 14. Block diagram of the fine frequency estimator.

to bring the maximum value of the frequency error down to 100 kHz (which, when normalized to the symbol rate of 25 Mbaud, corresponds to $4\cdot 10^{-3}$) in about 100 ms by using a normalized loop bandwidth of 10^{-4}.

An alternative method is described in [16], capable of handling very large frequency offset (larger than 25% of the symbol rate) at very low SNRs (lower than -2 dB).

4) Fine Carrier Frequency Recovery: For fine carrier frequency recovery, a pilot-based feedforward algorithm is proposed in [11], derived from the L&R technique [17] and modified in order to average the mean N point autocorrelation function $\sum_{m=1}^{N} R(m)$ over L consecutive pilot blocks before computing the argument function.

The algorithm block diagram is depicted in Fig. 14. The expression of the frequency estimate is

$$\hat{v}T = \frac{1}{\pi(N+1)} \arg\left\{ \sum_{l=1}^{L} \sum_{m=1}^{N} R_l(m) \right\} \tag{4}$$

where $R_l(m)$, for $m = 1,\ldots N$, are the N points of the autocorrelation vector, computed over the lth pilot symbol block, i.e.,

$$R_l(m) = \frac{1}{L_p - m} \sum_{k=m}^{L_p-1} z^{(p)}(k + lL_s) \cdot c^{(p)*}(k + lL_s) \cdot z^{(p)*}(k - m + lL_s) \cdot c^{(p)}(k - m + lL_s). \tag{5}$$

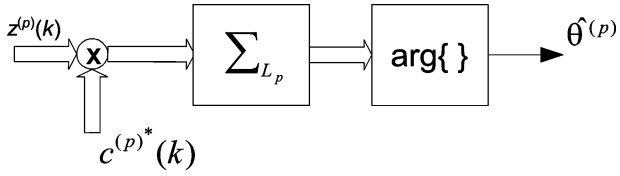

Fig. 15. FF ML phase estimator.

$L_p = 36$ is the number of symbols in a pilot block, and $L_s = 1476$ is the number of symbols between the start of two pilot blocks (see Section II-D).

Simulations [11] indicate that with $L = 1000$ (i.e., in about 60 ms at 25 Mbaud) and $N = 18$, the rms value of the residual normalized frequency error can be maintained below $5.3\cdot 10^{-5}$ (compatible with the requirements of the proposed phase recovery algorithm) for SNRs down to about 1 dB. No outliers have been recorded over long simulations at SNRs as low as -2 dB and with a frequency error of 100 kHz. Nevertheless, in this case the parameter L has to be increased to about 2500 (i.e., 150-ms delay) in order to get the required rms jitter.

5) Carrier Phase Recovery: The carrier phase-recovery algorithm has to cope with a residual carrier frequency error from the carrier frequency recovery unit as well as a strong phase noise (as defined in [3], Annex H8). For low-order modulations (QPSK and 8PSK) a very simple pilot-aided technique can be applied, which derives the phase trajectory over the data symbols by just linear interpolation of estimates performed over two consecutive pilot blocks. As the symbols

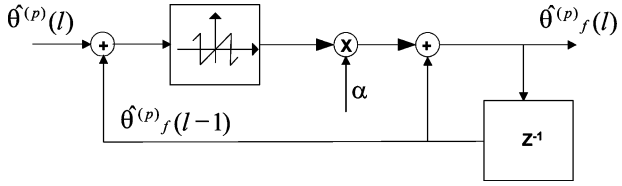

Fig. 16. The unwrapping algorithm.

transmitted over the pilots are known, the best estimator is the maximum likelihood (ML) estimator ([13, Ch. 5]). However, since the number of symbols in a pilot block L_p is short (36), in [11] a feedforward (FF) approach is also suggested in order to speed up the required estimation process. The phase estimate is carried out by collecting the L_p matched filter output samples $z^p(k)$ at a baud rate corresponding to the pilot blocks, and performing the following algebraic operations:

$$\hat{\theta}^{(p)} = \arg\left\{ \sum_{k=0}^{L_p-1} \left[c^{(p)}(k)\right]^* z^{(p)}(k) \right\}. \tag{6}$$

The algorithm gives just one estimate every pilot block, so if the carrier phase is actually time variant due to phase noise or an uncompensated carrier frequency error, the estimate made will be an average of the phase evolution during the pilot block. However, if L_p is small and the phase process relatively slow, the time variation property of the carrier phase can be neglected. Under this hypothesis and with relatively high SNRs, it can be shown (see [13, Ch. 5]) that (6) can be rewritten as

$$\hat{\theta}^{(p)} \cong \theta + N_I \tag{7}$$

with N_I being the zero-mean Gaussian noise contribution to the phase estimate, with variance

$$\sigma^2_{N_I} \cong \sigma^2_{\hat{\theta}^{(p)}} = \frac{1}{\frac{2L_pE_s}{N_0}} \tag{8}$$

which is independent of the modulation used in the pilot blocks. For very low SNRs a departure of the phase estimate variance from (8) is expected, even though simulations [11] indicate that for $L_p = 36$ the differences are very small down to SNR $= -6$ dB.

The FF ML estimator (6) provides a phase estimate in the interval $[-\pi, \pi]$, while the true carrier phase may grow beyond this range over a time interval separating two pilot blocks; to obtain a good estimation of the true carrier phase, an "unwrapping" technique is proposed in [11] and graphically represented in Fig. 16.

If the index "l" counts the number of pilot-based estimates, the final unwrapped pilot estimates $\hat{\theta}^{(p)}_f(l)$ are computed from $\hat{\theta}^{(p)}(l)$ as

$$\hat{\theta}^{(p)}_f(l) = \hat{\theta}^{(p)}_f(l-1) + \alpha \mathrm{SAW}\left[\hat{\theta}^{(p)}(l) - \hat{\theta}^{(p)}_f(l-1)\right] \tag{9}$$

where $\mathrm{SAW}[\Phi] \equiv [\Phi]^{+\pi}_{-\pi}$ is a saw-tooth nonlinearity that reduces Φ to the interval $[-\pi, \pi)$ and α is a weighting parameter in the range $0 < \alpha \leq 1$, which is set equal to one.

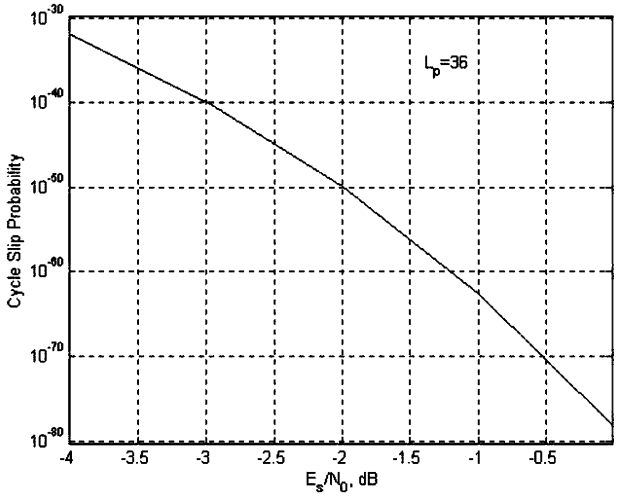

Fig. 17. Cycle slip probability of the phase unwrapping algorithm.

If the difference between the carrier phase in the current pilot block and the final estimate $\hat{\theta}^{(p)}_f(l)$ on the previous slot is less than π, the algorithm provides a good final unwrapped pilot phase estimate; otherwise, there is a cycle slip. This happens for example when, as a result of a residual carrier frequency offset $\Delta\nu$, the carrier phase grows linearly over two consecutive pilot blocks of more than π, i.e.,

$$\frac{2\pi\Delta\nu L_s}{R_s} \geq \pi \Rightarrow \frac{\Delta\nu}{R_s} \geq \frac{1}{2L_s}. \tag{10}$$

Equation (10) poses a limit on the maximum value of the residual normalized frequency error that the unwrapping algorithm can cope with without cycle slips. The longer the interval between pilots, the smaller the max sustainable frequency offset. For $L_s = 1476$ the max sustainable normalized carrier frequency error turns out to be $3.4 \cdot 10^{-4}$.

Equation (10) takes into account only the carrier frequency offset; when thermal noise is also considered, the cycle slip rate may increase. In particular, under the assumption of high SNRs, (7) indicates that the phase estimates coming out of the FF ML estimator are Gaussian and independent so that one could compute the probability that a cycle slip occurs as in [11].

$$\begin{aligned} P_{cs} &= \Pr\left\{\left|\theta^{(p)}(l) - \theta^{(p)}(l-1)\right| > \pi\right\} \\ &= 2\int_{\pi}^{\infty} \frac{1}{\sqrt{4\pi\sigma^2_{N_I}}} e^{-\frac{x^2}{4\sigma^2_{N_I}}} dx. \end{aligned} \tag{11}$$

Fig. 17 shows the cycle slip probability P_{cs} as a function of E_s/N_0 for $L_p = 36$, computed using (11). In order to have less than 1 cycle slip event per transmission hour, the probability of cycle slip has to be set to less than $L_s/(3600\ R_s)$, which corresponds to the inverse of the number of pilot block-based phase estimates per hour. For example, with $R_s = 25 \cdot 10^6$ and $L_s = 1476$, the requirement on P_{cs} is $16.4 \cdot 10^{-9}$, which is largely met for any value of the operating E_s/N_0 of DVB-S2.

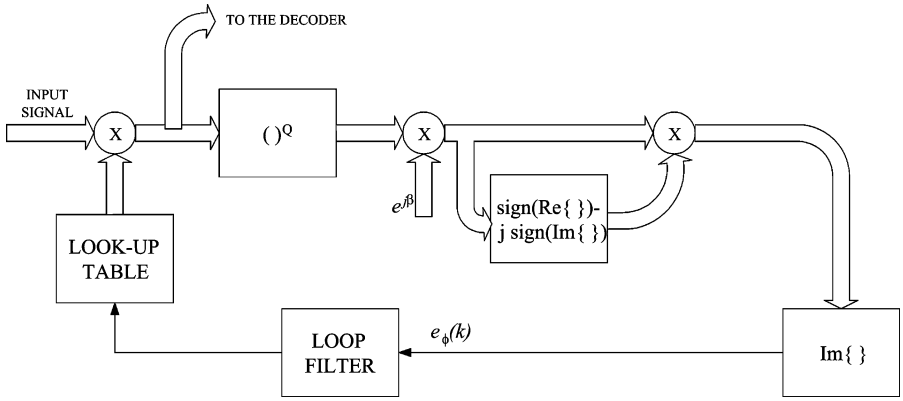

Fig. 18. Fine phase recovery unit.

Once the unwrapped FF-ML phase estimates are performed, linear interpolation between consecutive pilot-based estimates can be carried out.

Performance assessments have been carried out in [11], evaluating the rms phase error jitter in the presence of phase noise and with a normalized carrier frequency error of 10^{-4}, for 25-Mbaud transmission rate. The rms error decreases with the E_s/N_0 value, but it tends to reach a floor at about 3° for large values of E_s/N_0, because, even in the absence of noise, the phase estimator is not able to perfectly track the phase noise trajectory within the data portion of the pilot repetition period. The adoption of a Wiener filter interpolation technique over the data symbols could reduce this effect, but the expected performance improvements generally do not justify the added complexity. If the achieved performance is fully acceptable with QPSK and even with 8PSK, for high-order modulations like 16APSK and 32APSK the introduction of the fine phase recovery unit, (see Section III-A7) is advisable. Nevertheless, the phase noise masks as defined in [3] may be considered unduly critical for professional applications, where the cost of a better performance front-end oscillator is negligible.

6) Digital Automatic Gain Control: The decoder needs accurate soft information about the received symbol distance from the reference constellation points: a digital automatic gain control (DAGC) must adjust the level of the incoming symbols to the reference constellation. In [11] a data aided vector tracker is proposed, capable of operating in the presence of a frame-by-frame varying physical layer over a wide range of SNRs $(-2.5 < E_s/N_0 < 16\ \text{dB})$.

7) Fine Phase Recovery: Fine phase recovery is finally carried out for high-order and more phase-jitter-sensitive modulations (16APSK and 32APSK essentially), to further reduce the residual phase error of the coarse phase estimator. The algorithm proposed in [11] is the Qth power close-loop NDA phase synchronizer of Fig. 18, operating on the modulated data symbols.

The corresponding phase error detector has the following form:

$$e_\phi(k) = \text{Im}\left\{q(k)\left(\text{sign}\left[\text{Re}\left\{q(k)\right\}\right] - j\text{sign}\left[\text{Re}\left\{q(k)\right\}\right]\right)\right\} \tag{12}$$

where

$$q(k) = \begin{cases} [z(k)]^3 & \text{for 16APSK} \\ [z(k)]^4\, e^{j\frac{\pi}{4}} & \text{for 32APSK} \end{cases}. \tag{13}$$

Raising the 16APSK and 32APSK constellations to the 3rd and 4th power respectively (in the complex domain), transforms them into QPSK [12]. To maintain the same decision zones, a $\pi/4$ phase shift is required for 32APSK. The fine phase recovery unit works at the output of the coarse phase recovery unit, implementing the PA-LI algorithm, and its memory (loop filter) is reset once every pilot block. This greatly helps in reducing the probability of cycle slips under reasonable values. The digital AGC block is placed just before the fine carrier recovery unit in order to guarantee a precise setting of the loop bandwidth, as this is important in order to optimize the loop performance and minimize the system loss.

B. LDPC Decoding

LDPC decoding is based on an iterative exchange of information among bit nodes and check nodes (see Section II-B), to determine the transmitted bit values. The decoding starts by assigning the received channel values to all the outgoing edges from the corresponding bit node to its adjacent check nodes. Upon receiving that, the check nodes make use of the parity check equations to update the bit node information and sends it back. Each bit node then performs a soft majority vote among the information reaching it from adjacent check nodes. At this point, if the hard decisions on the bits satisfy all of the parity check equations, it means a valid codeword has been found and the process stops. Otherwise bit nodes go on sending the result of their soft majority votes to the check nodes. The decoding details are now described.

1) Initialization: Let x denote the transmitted binary phase shift keying (BPSK) symbol corresponding to a codeword bit, and y the noisy received symbol, $y = x + q$, where q is a Gaussian random variable with zero mean.

Let us assume that $x = +1$ when the transmitted bit is 0 and $x = -1$ when the transmitted bit is 1.

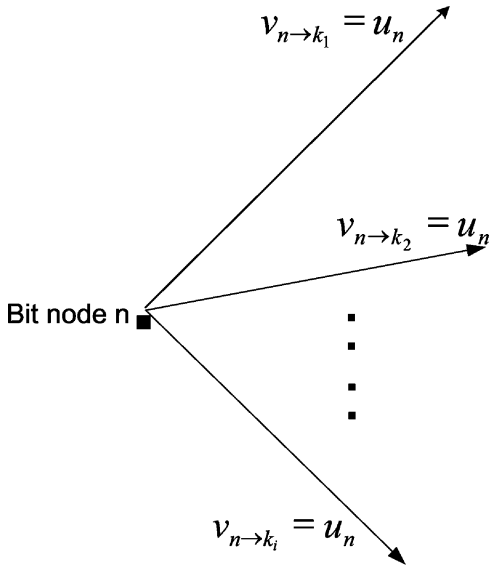

Fig. 19. Initialization of outgoing messages from bit nodes.

Let $u = \log(p(x = +1|y)/p(x = -1|y))$ denote the *a priori* log-likelihood ratio for the transmitted bit. The sign of u signals the hard decision on the transmitted bit, whereas the magnitude of u gives an indication of the reliability of the decision—the bigger the magnitude, the higher the reliability.

Decoding starts by assigning the *a priori* log-likelihood to all of the outgoing edges of every bit node

$$v_{n\to k_i} = u_n \quad \begin{matrix} n = 0, 1, \ldots, N-1 \\ i = 1, 2, \ldots, \deg(n) \end{matrix}, \tag{14}$$

where $v_{n\to k_i}$ denotes the message that goes from bit node n to its adjacent check node k_i, u_n denotes the *a priori* log-likelihood for bit n and N is the codeword size. The initialization process is also shown in Fig. 19.

2) Check Node Update: If $v_{n_1\to k}, v_{n_2\to k}, \ldots, v_{n_{dc}\to k}$ are the incoming messages to the check node k from its d_c adjacent bit nodes (see Fig. 20), the outgoing messages from the check node k back to d_c adjacent bit nodes $w_{k\to n_1}, w_{k\to n_2}, \ldots, w_{k\to n_{dc}}$ can be computed as

$$w_{k\to n_i} = g\left(v_{n_1\to k}, v_{n_2\to k}, \ldots, v_{n_{i-1}\to k}, v_{n_{i+1}\to k}, \ldots, v_{n_{dc}\to k}\right) \tag{15}$$

where

$$g(a,b) = \text{sign}(a)\cdot\text{sign}(b)\cdot\{\min(|a|,|b|)\} + LUT_g(a,b) \tag{16}$$

and

$$LUT_g(a,b) = \log\left(1+e^{-|a+b|}\right) - \log\left(1+e^{-|a-b|}\right). \tag{17}$$

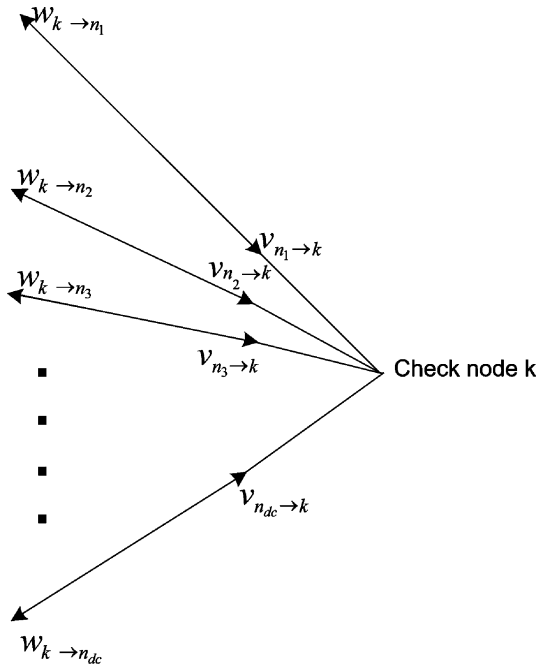

Fig. 20. Message update at check nodes.

In practice, the $LUT_g(.)$ function is implemented using a small look-up table. The g function with multiple inputs can be recursively computed, i.e.,

$$\begin{aligned} &g\left(v_{n_1\to k}, v_{n_2\to k}, \ldots, v_{n_{i-1}\to k}, v_{n_{i+1}\to k}, \ldots, v_{n_{dc}\to k}\right) \\ &\quad = g\left(g\left(v_{n_1\to k}, v_{n_2\to k}, \ldots, v_{n_{i-1}\to k}, \right.\right. \\ &\qquad \left.\left. v_{n_{i+1}\to k}, \ldots, v_{n_{dc-1}\to k}\right), v_{n_{dc}\to k}\right). \end{aligned} \tag{18}$$

Ignoring the small correction factor, i.e., $LUT_g = 0$, it is intuitive to understand check node computations; in fact

$$\begin{aligned} &\text{sign}\left(w_{k\to n_i}\right) = \text{sign}\left(v_{n_1\to k}\right)\cdot\text{sign}\left(v_{n_2\to k}\right)\cdot\ldots \\ &\cdot\text{sign}\left(v_{n_{i-1}\to k}\right)\cdot\text{sign}\left(v_{n_{i+1}\to k}\right)\cdot\ldots\cdot\text{sign}\left(v_{n_{dc}\to k}\right) \end{aligned} \tag{19}$$

and

$$\begin{aligned} \left|w_{k\to n_i}\right| = \min\left(\left|v_{n_1\to k}\right|, \left|v_{n_2\to k}\right|, \ldots, \left|v_{n_{i-1}\to k}\right|, \right. \\ \left.\left|v_{n_{i+1}\to k}\right|, \ldots, \left|v_{n_{dc}\to k}\right|\right). \end{aligned} \tag{20}$$

The first equality is merely a restatement of the fact that the hard decision on a certain bit is modulo-2 sum of all the other bits that participate in the same parity check equation, whereas the second equality states that the hard decision can only be as reliable as the least reliable bit in the modulo-2 sum.

3) Bit Node Update: If $w_{k_1\to n}, w_{k_2\to n}, \ldots, w_{k_{dv}\to n}$ are the incoming messages to the bit node n from its d_v adjacent check nodes (see Fig. 21), the outgoing messages

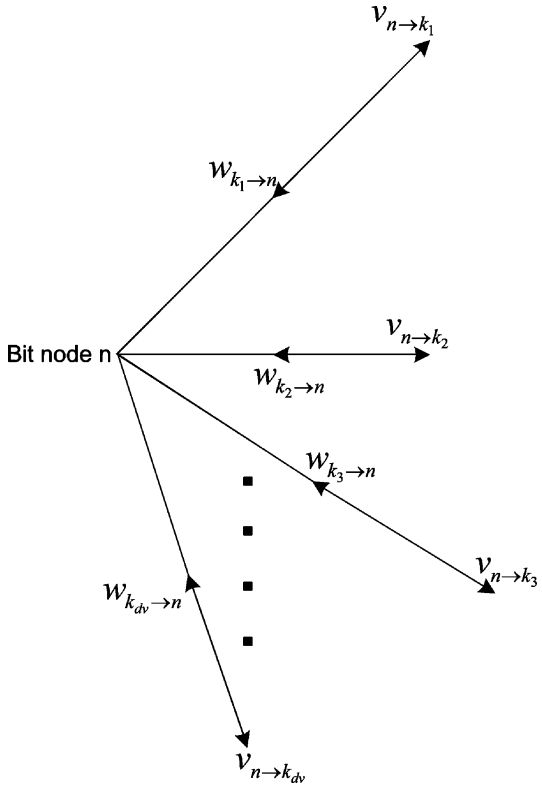

Fig. 21. Message update at bit nodes.

from the bit node n back to d_ν adjacent check nodes $v_{n\to k_1}, v_{n\to k_2}, \ldots, v_{n\to k_{dv}}$ can be computed as

$$v_{n\to k_i} = u_n + \sum_{j\neq i} w_{k_j\to n}. \tag{21}$$

Intuitively, this is a soft majority vote on the value of bit n, using all relevant information except $w_{k_i\to n}$.

4) Hard Decision Making: After the bit node updates, the hard decision can be made for each bit n by looking at the sign of $v_{n\to k_i} + w_{k_i\to n}$ for any k_i. If the hard decisions satisfy all the parity check equations, it means a valid codeword has been found, and therefore the process stops. Otherwise another check node/bit node update is performed. If no convergence is achieved after a predetermined number of iterations, the current output is given out and a decoding failure can be declared.

IV. The System Performance

Dependent on the selected code rate and modulation constellation, and assuming ideal demodulation, the system can operate, with a residual PER less than 10^{-7} in the AWGN channel, at signal-to-noise ratios from -2.4 dB using QPSK 1/4 to 16 dB using 32APSK 9/10, (see Fig. 22). The distance from the modulation-constrained Shannon limit ranges from 0.7 to 1.2 dB. The result is typically a 20%–35% capacity increase over DVB-S and DVB-DSNG under the same transmission conditions or, alternatively, 2–2.5 dB more robust reception for the same spectrum efficiency.

Fig. 22 also indicates examples of the useful bit rate capacity R_u achievable by the system in the different modulation/coding configurations, for a unit symbol rate R_s, i.e., $R_s = 1$ baud. The symbol rate R_s corresponds to the -3 dB bandwidth of the modulated signal, while $R_s(1+\alpha)$ corresponds to the theoretical total signal bandwidth after the modulator, with α representing the rolloff factor of the modulation. The use of narrower rolloff coefficients, $\alpha = 0.25$ and $\alpha = 0.20$, may allow a transmission capacity increase, but may also produce larger nonlinear degradations for single-carrier satellite operation.

When DVB-S2 is transmitted by satellite, quasi-constant envelope modulations, such as QPSK and 8PSK, are power efficient in the single-carrier-per-transponder configuration, since they can operate on transponders driven near saturation. 16APSK and 32APSK, which are inherently more sensitive to nonlinear distortions and would require quasi-linear transponders [i.e., with larger output-back-off (OBO)] may be improved in terms of power efficiency by using nonlinear compensation techniques in the uplink station (ref. Appendix A).

The DVB-S2 system may be used in "single-carrier-per-transponder" or in "multicarriers-per-transponder" [frequency-division multiplexing (FDM)] configurations.

In [11] results are reported of simulations, carried out by E. Casini *et al.*, of the single-carrier-per-transponder configuration, using the satellite channel models and phase noise mask given in [3] (i.e., nonlinearized TWTA, phase noise PN relevant to consumer LNBs, dynamic precompensation techniques on the modulator—see Appendix A). The simulated chain is the one described in Sections II (transmitting side) and III (receiving side). Figs. 23 and 24 show the performance of the four modulation schemes in AWGN and nonlinear channels (assuming optimum IBO), with and without performance losses due to nonperfect synchronization and phase noise (PN).

Table 1 summarizes the total performance degradations of the DVB-S2 system obtained by computer simulations under various conditions: with and without dynamic predistortion in the uplink station, with and without phase noise/synchronization losses. C_{SAT} is the un-modulated carrier power at high-power-amplifier (HPA) saturation, OBO is the measured power ratio (in decibels) between the unmodulated carrier at saturation and the modulated carrier (after OMUX). The total loss is computed by adding the nonlinear power losses (i.e., the measured OBO) to the distortion losses (for instance, E_s/N_0 distances in decibels between the AWGN and nonlinear channel curves in Figs. 23 and 24, at BER $= 10^{-5}$).

The figures show the large advantage offered by the use of dynamic predistortion for 16APSK and 32APSK. The large phase noise degradations quoted for APSK, and in particular for 32APSK, can be considered as pessimistic, since they refer to consumer-type LNBs while, for professional applications, better front-ends may be adopted at negligible additional cost.

In FDM configurations, where multiple carriers occupy the same transponder, the transponder must be kept in the

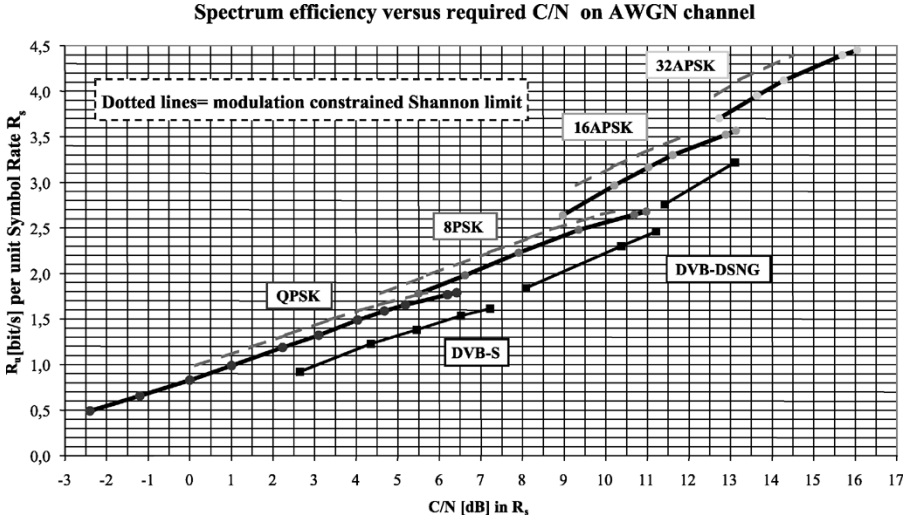

Fig. 22. Required E_s/N_0 versus spectrum efficiency in the AWGN channel (ideal demodulation).

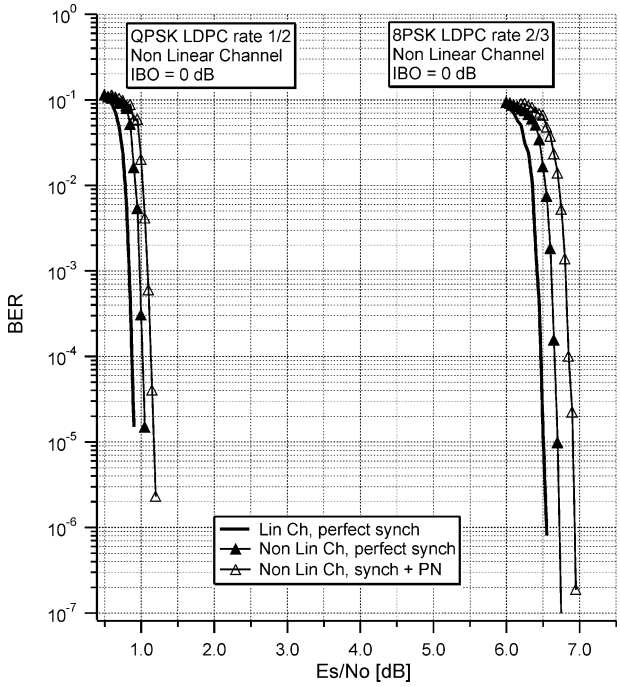

Fig. 23. Comparison of BER curves for QPSK 1/2 and 8PSK 2/3 in AWGN and nonlinear channels (with and without synch losses).

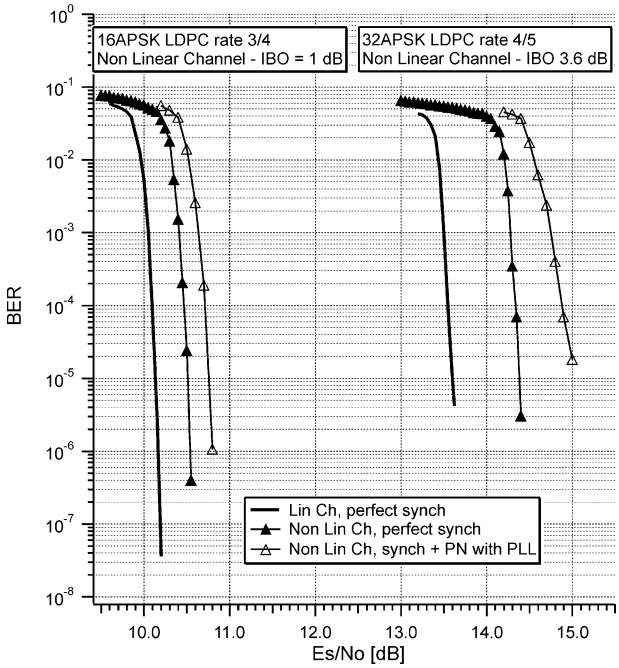

Fig. 24. Comparison of BER curves for 16 APSK 3/4 and 32APSK 4/5 in AWGN and nonlinear channels (with and without synch losses).

quasi-linear operating region (i.e., with large OBO) to avoid excessive intermodulation interference between signals. In this case the AWGN performance figures may be adopted for link budget computations.

V. Examples of Possible Use of the System

The following examples give some possible applications of the DVB-S2 system, showing the advantages offered by its excellent performance and flexibility with respect to the first-generation standards DVB-S and DVB-DSNG.

First of all, the case of TV broadcasting is analyzed: Table 2 compares DVB-S2 and DVB-S broadcasting services via 36 MHz (at -3 dB) satellite transponders, with satellite EIRPs of 53.7 dBW at the service area contour, using 60-cm receiving antenna diameters. The required C/N of the two systems, DVB-S and DVB-S2, have been balanced by exploiting different transmission modes (constant

Table 1
C_{SAT}/N Loss [dB] on the Satellite Channel

Transmission Mode	No pre-distortion No Phase Noise	Dynamic pre-distortion No Phase Noise	Dynamic pre-distortion Phase Noise
QPSK ½	0.6 (OBO=0.3)	0.5 (IBO=0; OBO=0.4)	0.6
8PSK 2/3	1.0 (OBO=0.4)	0.6 (IBO=0;OBO=0.4)	0.9
16APSK ¾	3.2 (OBO=1.7)	1.5 (IBO=1.0; OBO=1.1)	1.8
32APSK 4/5	6.2 (OBO=3.7)	2.8 (IBO=3.6; OBO=2.0)	3.5

Table 2
Example Comparison Between DVB-S and DVB-S2 for TV/HDTV Broadcasting

Satellite EIRP (dBW)		53.7
System	DVB-S	DVB-S2
Transmission mode	QPSK 7/8	8PSK 2/3
Symbol-rate (Mbaud)	27.5 (α=0.35)	29.7 (α=0.25)
C/N (in 27.5 MHz) (dB)	7.8	7.8
Useful bit-rate (Mbit/s)	44.4	58.8 (gain=32%)
Number of SDTV programmes	10 MPEG-2 20 MPEG-4	13 MPEG-2 26 MPEG-4
Number of HDTV programmes	2 MPEG-2 5 MPEG-4	3 MPEG-2 6 MPEG-4

coding and modulation) and by fine tuning the DVB-S2 rolloff factor and symbol-rate. The results confirm the capacity gain of DVB-S2 over DVB-S, exceeding 30%. Furthermore, by combining DVB-S2 and MPEG-4/H.264 coding, an impressive number of 26 SDTV channels per transponder are obtained, thus dramatically reducing the cost per channel of the satellite capacity. The combination of DVB-S2 and new MPEG-4 coding schemes can favor the introduction of new HDTV services, with an adequate number of programs per transponder (e.g., 6), reducing the satellite capacity cost increase with respect to current SDTV services. The example video coding bit rates are: 4.4 Mb/s (SDTV) and 18 Mb/s (HDTV) using traditional MPEG-2 coding, or 2.2 Mb/s (SDTV) and 9 Mb/s (HDTV) using MPEG-4 advanced video coding (H.264) systems which the DVB Project is currently defining for future applications [5].

The DVB-S2 system may also deliver broadcasting services over multiple TSs, providing differentiated error protection per multiplex. A typical application is broadcasting of a highly protected multiplex for SDTV, and of a less protected multiplex for HDTV. Assuming a symbol rate of 27.5 Mbaud and using 8PSK 3/4 and QPSK 2/3, 40 Mb/s could be available for two HDTV programs and 12 Mb/s for two to three SDTV programs, with a difference in C/N requirements of around 5 dB.

When DVB-S2 is used for interactive point-to-point applications like IP unicasting, its gain over DVB-S can become much greater, if ACM is adopted. Fig. 25 shows the scheme of an ACM satellite link, comprising the ACM gateway (GW), the DVB-S2 ACM modulator, the uplink station, the satellite, and the satellite receiving terminal (ST) connected to the ACM GW via a return channel. The DVB-S2 ACM modulator operates at constant symbol rate, since the available transponder bandwidth is assumed to be constant. ACM is implemented by the DVB-S2 modulator by transmitting, in time-division multiplex (TDM), a sequence of frames, where the coding and modulation format may change frame-by-frame. Therefore, service continuity is achieved, during rain fades, by reducing user bits while increasing, at the same time, the FEC redundancy and/or modulation ruggedness. Physical layer adaptation is achieved as follows.

1) Each ST measures the channel status (available C/N+I) and reports it via the return channel to the GW.
2) The ST reports are taken into account by the GW while selecting the assigned protection level for data packets addressed to the ST.
3) In order to avoid information overflow during fades, a user bit rate control mechanism should be implemented, adapting the offered traffic to the available channel capacity.

The network configuration depicted in Fig. 25 allows us to recover the so-called clear sky margin, typically 4–8 dB of extra power transmitted by conventional constant coding and modulation (CCM) systems, so that the system works properly in the presence of heavy rain fades. In [4, Annex D], examples are given of the gain offered by ACM, which can double or even triple the average satellite throughput, thus dramatically reducing the service cost. Furthermore it must be considered that the ACM gain versus CCM increases for critical propagation conditions. Therefore, ACM is fundamental for higher frequency bands (e.g., *Ka*-band) and for tropical climatic zones.

ACM functionality is also interesting for professional applications, as it allows increasing the gain offered by DVB-S2 by over 30%. Let us consider first the examples of TV contribution services using large transmitting and receiving stations to access a typical 36-MHz transponder with four FDMA signals. Using the DVB-DSNG standard and 16QAM 3/4 mode, four TV contribution signals each at 18.5 Mb/s may be allocated in the transponder using 7 m transmitting/receiving antenna diameters. Using DVB-S2, 16APSK 5/6 and rolloff equal to 0.2, the information rate of each link can be increased to 24.75 Mb/s, thus confirming a bit rate gain of DVB-S2 over DVB-DSNG of more than 30%. On the other hand, keeping the same bit rate as DVB-DSNG, the better performance of DVB-S2 may be used to significantly decrease the dimensions of the transmitting/receiving antennas (down to 4.5-m diameter). With the same 4.5-m antennas, but adding the ACM functionality of DVB-S2, the useful bit rate could be increased again to around 24 Mb/s, at least for a large percentage of the transmitting time (i.e., under good propagation conditions).

The advantages of DVB-S2 and ACM are also evident for DSNG services. For example, in a 9-MHz satellite bandwidth slot, a DSNG van equipped with 1.2-m antenna may transmit using DVB-S2 19.8 Mb/s in clear sky conditions (16APSK 2/3, rolloff $= 0.2$) and switch to 14.85 Mb/s under heavy fading conditions (8PSK 2/3). For the sake of comparison, DVB-DSNG standard with QPSK 7/8 would allow the transmission of 10.7 Mb/s only.

As a last example, let us consider a very small emergency DSNG station (a so-called fly-away station), with a 90-cm antenna and only 12-W HPA power. Using DVB-S2 and ACM, a bit rate of 9.9 Mb/s (QPSK 2/3, rolloff $= 0.2$) would be available in clear sky conditions, 8.9 Mb/s (QPSK 3/5) under typical propagation conditions, to be reduced to 3.68 Mb/s (QPSK1/4) only under very critical link conditions (happening for a small percentage of the time). This would still offer an acceptable picture quality using MPEG-2 video coding, and excellent quality using the new MPEG-4

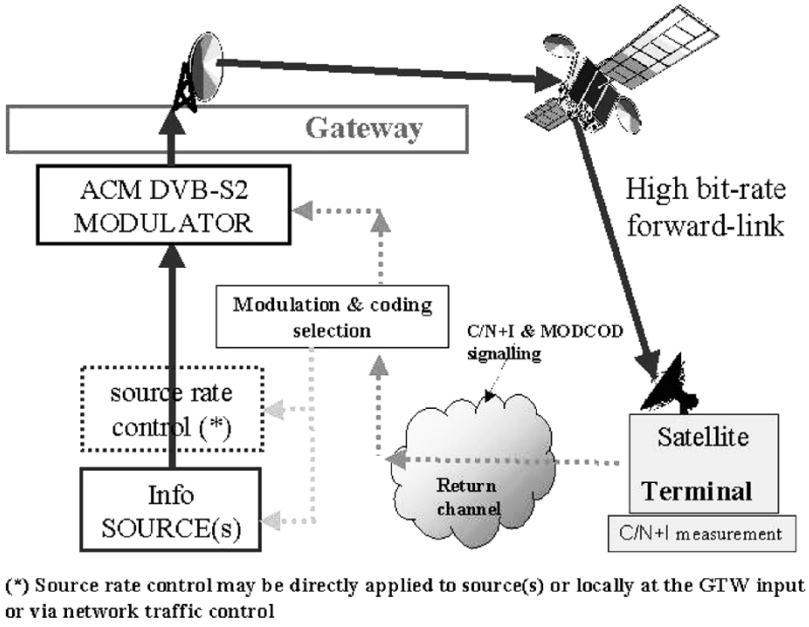

Fig. 25. Block diagram of a DVB-S2 ACM link.

encoders. DVB-S (QPSK1/2) would instead require a 5 dB more powerful station to offer a constant bit rate of 6.1 Mb/s.

VI. Conclusion

In this paper we have presented the main characteristics of the DVB-S2 system, and described the main modulation/demodulation algorithms for a modem implementation, including receiver synchronization. The algorithms have been presented in detail and analyzed by means of theory and computer simulations, including real-channel distortions such as nonlinear satellite channel (IMUX, TWTA, OMUX), predistortion algorithms in the uplink station, and front-end phase noise.

End-to-end performance simulation results have been shown with all the designed modulation/demodulation algorithms active. Performance losses with respect to the ideal case have been computed, showing very limited penalties with respect to the ideal case. Results show that high-order modulation schemes up to 32APSK can be successfully used without excessive penalties.

The DVB Project does not see DVB-S2 replacing DVB-S in the very short term for conventional TV broadcasting applications. Millions of DVB-S decoders are already operating reliably, contributing to successful digital satellite businesses around the world. New applications are being envisaged for satellite services such as the delivery of consumer HDTV and the delivery of IP-based services, where DVB-S2 may find a rapid application. Two examples can highlight the revolution we have in front of us. Combining DVB-S2 and new video and audio coding schemes (e.g., MPEG-4/H.264), up to 20–25 SDTV or 5–6 HDTV programs may be broadcast in a conventional *Ku*-band 36-MHz transponder (while still being able to decode current DVB-S services). In the area of interactive data services, the DVB-S2 ACM tool may halve the satellite capacity costs, and thus it may relaunch the perspectives of fast Internet by satellite, at least in rural areas and developing countries, where terrestrial xDSL infrastructures are not available. In these new application areas, DVB-S2 will do what DVB-S could never have done.

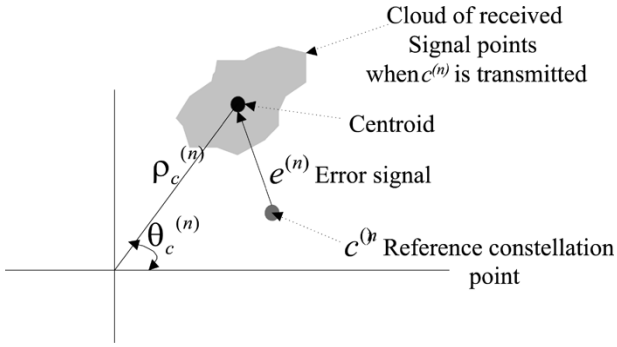

Fig. 26. Pictorial view of the static predistortion algorithm.

Appendix A.
Modulator Precompensation Algorithms

APSK modulation is characterized by constellation points lying on concentric circles. Two main kinds of impairment (pictorially represented in Fig. 26) affect it over nonlinear channels (see [3] for typical AM/AM and AM/PM satellite TWTA amplifier).

1) The constellation centroids warping, due to nonlinear characteristics of the AM/AM and AM/PM HPA. The centroid is the compilation of received constellation cluster centers of mass, conditioned to each constellation point. The warping effect is responsible for a reduction in the distance among APSK rings (AM/AM compression) and a differential phase rotation among them (AM/PM differential phase).

2) The clustering effect due to the intersymbol interference (ISI) experienced at the demodulator matched-filter output. The demodulator square root raised cosine (SRRC) filter does not perfectly match the received signal, due to the combination of the signal band-limiting (which introduces memory in the channel), the IMUX filter linear distortion, the HPA memory-less nonlinearity, and the OMUX linear filter distortions. The result is a nonlinear channel with memory.

Two kinds of predistortion techniques can be considered for APSK: "static" and "dynamic."

The static predistortion technique simply consists in modifying the APSK constellation points to minimize the centroids distance of the demodulator matched-filter samples from the "wanted" reference constellation.

The static precompensation is preferably performed off-line in the absence of AWGN, once the satellite channel characteristics are known. The static predistortion is able to correct for the constellation warping effects but it is not able to compensate for the clustering phenomenon.

The dynamic predistortion algorithm takes into account the memory of the channel that is conditioning the predistorted modulator constellation, not only for the currently transmitted symbol but also for the $(L-1)/2$ preceding and $(L-1)/2$ following symbols.

In [11] a dynamic predistortion algorithm is proposed which minimizes the total link degradation.

ACKNOWLEDGMENT

The authors would like to thank the members of the DVB-S2 Ad Hoc Group of the DVB Technical Module, for their excellent contributions during the system design and the provision of many simulation results presented throughout this paper. In particular, we wish to acknowledge Dr. M. Eroz, Dr. F.-W. Sun, Dr. L.-N. Lee, and Dr. Y. Jiang of Huges Network Systems (HNS); and Dr. E. Casini, Dr. R. De Gaudenzi, Dr. A. Ginesi, Dr. R. Rinaldo, and Dr. M. Vazquez-Castro of the European Space Agency (ESA).

REFERENCES

[1] *Digital video broadcasting (DVB); Framing structure, channel coding and modulation for 11/12 GHz satellite services*, EN 300 421 (V1.1.2), European Telecommunications Standards Institute (ETSI).

[2] *DVB: Framing structure, channel coding and modulation for DSNG and other contribution applications by satellite*, EN 301 210, European Telecommunications Standards Institute (ETSI).

[3] *Digital video broadcasting (DVB); Second generation framing structure, channel coding and modulation systems for broadcasting, interactive services, news gathering and other broad-band satellite applications*, EN 302 307, European Telecommunications Standards Institute (ETSI).

[4] "Digital video broadcasting (DVB); User guidelines for the second generation system for broadcasting, interactive services, news gathering and other broad-band satellite applications (DVB-S2)," European Telecommunications Standards Institute (ETSI), TR 102 376.

[5] "Digital video broadcasting (DVB); Implementation guidelines for the use of MPEG-2 systems, video and audio in satellite, cable and terrestrial broadcasting applications," European Telecommunications Standards Institute (ETSI), TR 101 154.

[6] U. Reimers and A. Morello, "DVB-S2, the second generation standard for satellite broadcasting and unicasting," *Int. J. Satell. Commun. Network.,* vol. 22, no. 3, May–Jun. 2004.

[7] R. Gallager, "Low density parity check codes," *IRE Trans. Inf. Theory,* vol. IT-8, pp. 21–28, Jan. 1962.

[8] D. J. MacKay and R. M. Neal, "Good codes based on very sparse matrices," in *Proc. 5th IMA Conf.* 1995, pp. 100–111.

[9] ——, "Near Shannon limit performance of low density parity check codes," *Electron. Lett.,* vol. 33, no. 6, pp. 457–45, Mar. 1997.

[10] M. Eroz, F.-W. Sun, and L.-N. Lee, "DVB-S2 low density parity check codes with near Shannon limit performance," *International Journal on Satellite Communication Networks,* vol. 22, no. 3, May–June 2004.

[11] E. Casini, R. De Gaudenzi, and A. Ginesi, "DVB-S2 modem algorithms design and performance over typical satellite channels," *Int. J. Satell. Commun. Network.,* vol. 22, no. 3, May–Jun. 2004.

[12] R. De Gaudenzi, A. Guillen i Fabregas, and A. Martinez Vicente, "Turbo-coded APSK modulations for satellite broadcasting—Part II: End-to-end performance," *IEEE Trans. Wireless Commun.,* 2004, submitted for publication.

[13] U. Mengali and A. N. D'Andrea*, Synchronization Techniques for Digital Receivers*. New York: Plenum, 1997.

[14] M. Oerder and H. Meyr, "Digital filter and square timing recovery," *IEEE Trans. Commun.,* vol. COM-36, no. 5, pp. 605–612, May 1988.

[15] F. M. Gardner, "A BPSK/QPSK timing-error detector for sampled receivers," *IEEE Trans. Commun.,* vol. COM-34, no. 5, pp. 423–429, May 1986.

[16] F.-W. Sun, Y. Jiang, and L.-N. Lee, "Frame synchronization and pilot structure for DVB-S2," *Int. J. Satell. Commun. Network.,* vol. 22, no. 3, pp. 319–339, May–Jun. 2004.

[17] M. Luise and R. Reggiannini, "Carrier frequency recovery in all digital modems for burst mode transmissions," *IEEE Trans. Commun.,* vol. COM-43, no. 2/3/4, pp. 1169–1178, Feb./Mar./Apr. 1995.

[18] R. Rinaldo, M. Vazquez-Castro, and A. Morello, "DVB-S2 ACM modes for IP and MPEG unicast applications," *Int. J. Satell. Commun. Network.,* vol. 22, no. 3, pp. 367–399, May–Jun. 2004.

[19] S. Cioni, R. De Gaudenzi, and R. Rinaldo, "Adaptive coding and modulation for the forward link of broad-band satellite networks," presented at the Globecom 2003 Conf., San Francisco, CA.

[20] E. Chen, J. L. Koslov, V. Mignone, and J. Santoru, "DVB-S2 backward-compatible modes: a bridge between the present and the future," *Int. J. Satell. Commun. Network.,* vol. 22, no. 3, pp. 341–365, May–Jun. 2004.

[21] R. Rinaldo and R. De Gaudenzi, "Capacity analysis and system optimization for the forward link of multi-beam satellite broadband systems exploiting adaptive coding and modulation," *Int. J. Satell. Commun. Network.,* vol. 22, no. 3, pp. 281–318, May–Jun. 2004.

[22] C. Weck, "Hierarchical modulation—the transmission of two independent DVB-T multiplexes on a single TV frequency," *EBU Tech. Rev.,* no. 294, Apr. 2003.

[23] A. Morello and V. Mignone, "New DVB standard for DSNG—and contribution satellite links," *EBU Tech. Rev.,* no. 277, Autumn 1998.

Alberto Morello received the degree in electronic engineering and the Ph.D. degree from the Politecnico di Torino, Turin, Italy , in 1982 and 1987, respectively.

He joined the RAI Research Centre, Turin, in 1984, where he became Head of the Digital Communication Laboratory in 1996 and finally Director in 1999. He was engaged in research on advanced digital modulation and coding techniques for television and sound broadcasting, as well as in the development of new multimedia and datacast services oriented to the user's set-top box or personal computer. He had a primary role in the RAI digital HDTV experiments via Olympus satellite (Italia '90), and in the definition of the DVB systems for

digital multiprogram TV broadcasting by satellite (ETS 300 421 standard) and on the terrestrial channels (ETS 300 744 standard). Furthermore, he was the chairman of the DVB group which defined the DVB-DSNG system, and is now leading the DVB-S2 group for the second generation DVB-satellite system. He is author of technical/scientific articles on leading reviews like IEEE Transactions and the EBU Technical Review, and regularly contributes to national and international Conferences.

Dr. Morello is member of EBU and CEPT Groups, and participated to a number of European Research and Development Projects, including DVB.

Vittoria Mignone was born in 1966. She received the Laurea in Ingegneria Elettronica degree from Politecnico di Torino, Turin, Italy in 1990.

In 1991, in cooperation with the Electronic Department of Politecnico di Torino, she was engaged in studies on satellite broadcasting on behalf of the National Research Council. Since 1992, she has been with the RAI Research Centre, Turin, involved in the studies for the definition of the European Telecommunications Standards Institute (ETSI) Standards for digital television broadcasting by satellite, cable, terrestrial channels, and DSNG. Her current activities are in the field of advanced digital modulation and channel coding techniques for satellite and terrestrial transmissions. She is the author of several technical papers.